Chinese Chemical Letters 31 (2020) 769–773

Contents lists available at ScienceDirect

Chinese Chemical Letters

journal homepage: www.elsevier.com/locate/cclet

Communication

Blood compatible heteratom-doped carbon dots for bio-imaging of human umbilical vein endothelial cells

Jian Zhong[a,c], Xinmian Chen[a], Miaoran Zhang[b], Chaoxin Xiao[c], Lulu Cai[a,*], Waleed Ali Khan[b], Kaixuan Yu[b], Jiayi Cui[b], Lin He[a,*]

[a] Personalized Drug Therapy Key Laboratory of Sichuan Province, Department of Pharmacy, Sichuan Provincial People's Hospital, School of Medicine, University of Electronic Science and Technology of China, Chengdu 610072, China
[b] State Key Laboratory of Heavy Oil Processing, Beijing Key Laboratory of Biogas Upgrading Utilization, College of New Energy and Materials, China University of Petroleum (Beijing), Beijing 102249, China
[c] State Key Laboratory of Biotherapy and Cancer, West China Hospital, Sichuan University and Collaborative Innovation Center, Chengdu 610041, China

ARTICLE INFO

Article history:
Received 26 November 2019
Received in revised form 2 January 2020
Accepted 3 January 2020
Available online 11 January 2020

Keywords:
Carbon dots
Fluorescent
Cell imaging
Erythrocyte
Blood compatibility

ABSTRACT

Carbon dots have unique advantages in biological applications owing to their excellent optical properties. However, the biosafety evaluation of carbon dots has limitations owing to cytotoxicity *in vitro*, and there is little pre-safety evaluation before *in vivo* and clinical applications. Whether the carbon dots are or not suitable for applications *in vivo*, evaluation analysis can be made based on hemolysis and changes in erythrocyte morphology. In this work, a green fluorescent N, S-doped carbon dots (N, S-CDs) were obtained by hydrothermal method, tobias acid, and *m*-phenylenediamine as precursors. N, S-CDs not only possessed excellent dispersibility, uniform particle size, high quantum yield (37.2%) and stable photoluminescence property but also retain their photostability and strong fluorescence intensity in the acid/alkaline solutions, different ionic strengths (NaCl) and under 365 nm UV illumination. Moreover, the N, S-CDs displayed low cytotoxicity and high cellular uptake efficiency in human umbilical vein endothelial cells (HUVEC) and excellent blood compatibility to the erythrocyte. It is foreseeable that N, S-CDs could be further studied as a promising biological imaging agent *in vivo*.

In recent years, carbon dots with fluorescence have become an emerging nano-material, thus attracting extensive research in the biomedicine field [1–3]. Owing to their advantages in small size, low production cost, good water dispersibility, superior optical properties, and excellent biocompatibility, carbon dots have shown encouraging results in multiple field applications including bioimaging, disease diagnosis, drug delivery, optoelectronics, energy conversion and photocatalysis [4–7]. Compared with other fluorescent materials such as metals and polymers, carbon dots, a material without toxic heavy metal ions, have much less toxicity in medical treatments [8] and overcome the shortcomings of other organic dyes (*e.g.*, photobleaching) [9].

However previous reports suggested that carbon dots still have some shortcomings in multiple field applications. Firstly, most carbon dots' emission spectra are mainly concentrated in the short-wave region (blue-light region), not in the long-wave region (green-light and red-light), the long-wave light can penetrate tissue more easily [10–13]. Also, carbon dots exhibit the disadvantage of low quantum yield as fluorescent imaging agents. To improve their fluorescent properties, much research has been conducted, for instance, doping of CDs with heteroatoms nitrogen, sulfur, and phosphorus [14–16]. Secondly, the lack of hydrophilic groups (phosphate, sulfonate or polyhydroxyl moieties) results in poor solubility and optical instability of carbon dots in solutions [17]. Thirdly, many clinical applications, such as bioimaging, disease diagnosis and drug delivery, are limited due to the hemolysis and endothelial toxicity attributes of carbon dots [10,15,18]. Liu *et al.* reported that unmodified CDs-PDMA80 can cause more than 10% hemolysis and lead to circulatory system disorder and even fatal toxicity, thus limiting the application of CDs-PDMA80 in gene delivery [19,20]. Therefore, carbon dots possessing long-wave emission spectra, good solubility, photostability and excellent biocompatibility *in vivo* are urgently required. In this work, we reported a kind of fluorescence-emitting N, S-doped carbon dots (N, S-CDs) by mixing nitrogen elements-equipped *m*-phenylenediamine and sulfur elements-equipped tobias acid together. The amino group of *m*-phenylenediamine could increase the solubility of N, S-CDs in aqueous solution.

* Corresponding authors.
E-mail addresses: cailulu@med.uestc.edu.cn (L. Cai), helin514@126.com (L. He).

https://doi.org/10.1016/j.cclet.2020.01.007

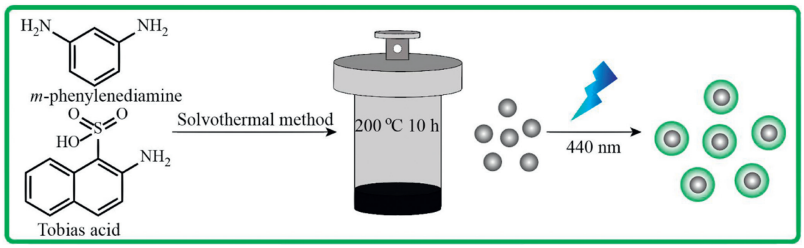

Scheme 1. Synthetic route of N, S-CDs.

Additionally, tobias acid and *m*-phenylenediamine provided S and N elements for CDs respectively, resulting in excellent photostability and improved quantum yield (QY) (37.2%). N, S-CDs displayed excellent photostability in acidic/alkaline solutions, enabling N, S-CDs a promising fluorescent imaging agent in the biological field. *In vitro* evaluation, N, S-CDs showed low cytotoxicity, high cellular uptake efficiency. Furthermore, N, S-CDs demonstrated good biocompatibility with erythrocytes. The N, S-CDs we reported have the characteristics of simple preparation procedure and excellent biocompatibility, suggesting that N, S-CDs have broad prospects in the biological field.

Scheme 1 showed the fabrication process of N, S-CDs. The morphology of N, S-CDs was obtained by transmission electron microscopy. The results were shown in Fig. 1a, N, S-CDs were uniformly dispersed nanospheres with a particle size of 2.59 ± 0.76 nm having well-resolved lattice structure with a *d* interval of 0.14 nm. To evaluate the functional component of N, S-CDs more accurately, X-ray photoelectron spectroscopy (XPS) was employed and results were shown in Fig. 1b. The two intensity peaks of the XPS spectrum were attributed to C 1s (284.80 eV) and O 1s (531.27 eV) respectively. And the XPS spectrum also showed that N, S-CDs contain N and S elements with the peaks at 397.73 eV (N 1s) and 168.99 eV (S 2p) respectively. The contents of C, N, O, and S were 50.15%, 0.75%, 48.58% and 0.52% respectively and were shown in Table S1 (Supporting information). As we can observe from Fig. 1c, the high-resolution C 1s spectra exhibited four peaks, and the four peaks separately represented sp^2 carbons (C-C/C = C, 284. 8 eV), sp^3 carbon (C-O/C-N, 286.58 eV), and carbonyl carbons (C=O, 288.42 eV; COOH, 289.4 eV); The O 1s spectra contained three peaks located at 531.28 eV, 531.47 eV and 535.5 eV (Fig. 1d), which were respectively attributed to C = O, C-O and COOH [21]. The high-resolution N 1s spectra showed a single peak (Fig. 1e), which was located at 398.56 eV and attributed to pyridinic N [22]; the high-resolution S 2p spectra also possessed only one peak (Fig. 1f), representing C-SO_X-C [23,24].

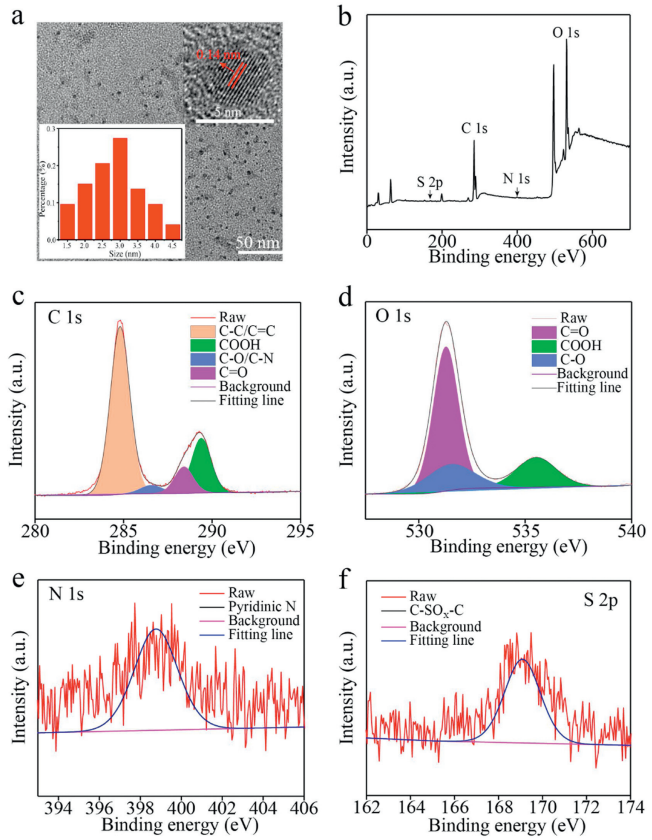

Fig. 1. (a) Transmission electron microscope (TEM) image of N, S-CDs. (b) X-ray photoelectron spectroscopy (XPS) of N, S-CDs. (c) High resolution C 1s. (d) High resolution O 1s. (e) High resolution N 1s. (f) High resolution S 2p.

To evaluate functional groups of N, S-CDs, Fourier transform infrared (FT-IR) spectrum was employed and the results were described in Fig. 2a. A broad absorption peak at 3381 cm^{-1} indicated the presence of OH and NH_2 on the surface of N, S-CDs and the weak absorption peak at about 2900 cm^{-1} implied the stretching and bending vibration of C–H [25]. Meanwhile, the absorption peak located at 1448 cm^{-1} represented the stretching vibration of C=C bonds, the absorption peak bulged out at 1629 cm^{-1} are assigned to C=O (carbonyl). The stretching vibration of C—N bonds' absorption peak as indicated by the sharp band at 1347 cm^{-1} and the bands at 1145 cm^{-1} denoted stretching vibration of C—O bonds. According to the FT-IR spectrum, the N, S-CDs consisted of aromatic rings, hydrophilic amino and carboxyl groups. Owing to the presence of these hydrophilic groups, the N, S-CDs possessed good water solubility.

The absorption and optical properties of N, S-CDs were analyzed by UV spectroscopy as well as excitation and emission spectroscopy. The results in Fig. 2b showed that N, S-CDs had absorption peaks at 255 nm and 290 nm which were assigned to the π-π^* transition of aromatic sp^2 and the n-π^* electronic transitions respectively. The absorption peaks at 340 nm were attributed to n-π^* transition of C=O and C=N [26]. While the broader and less absorptive absorption peaks at 340 nm and 440 nm represented the absorption wavelength of the N, S-CDs surface and the subsequent fluorescence excitation wavelength, respectively. The emission wavelength of N, S-CDs was found to be around 405 nm and were mainly present in the blue-light region (the result is not shown) when excited under a 340 nm wavelength, which caused limited use of N, S-CDs in biological applications. However, when excited with 440 nm ultraviolet light, the N, S-CDs solution could emit obvious green fluorescence (around 520 nm), which was valuable for biological applications. The optical characteristics of N, S-CDs were further studied by observing the emission spectra under different excitations. The fluorescence of N, S-CDs possessed stronger excitation wavelength which then ultimately became weaker when the excitation light altered from

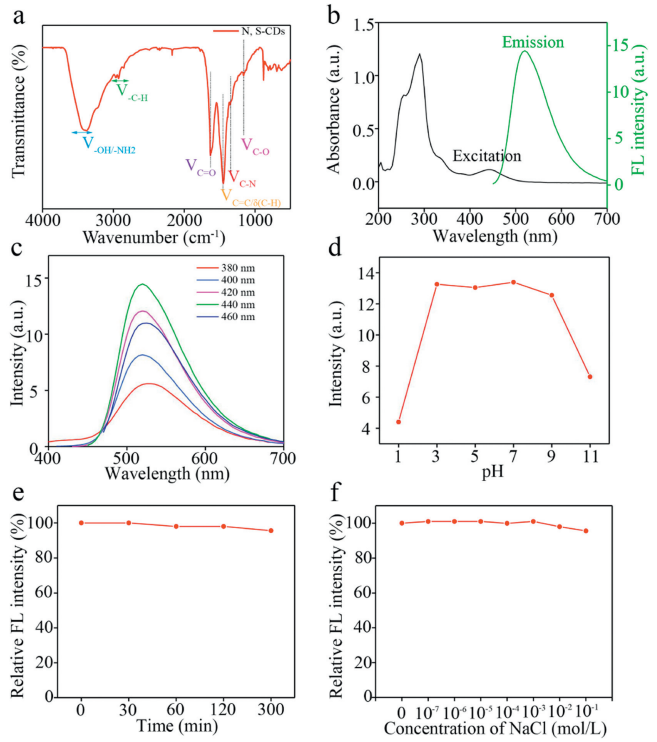

Fig. 2. (a) Fourier transform infrared (FTIR) spectrum of N, S-CDs. (b) UV–vis absorption spectrum of N, S-CDs. (c) Photoluminescence excitation spectra of N, S-CDs. (d) Fluorescent intensity of N, S-CDs under different pH values. (e) Fluorescence intensity of N, S-CDs at different time under 365 nm UV illumination (f) Fluorescence intensity of N, S-CDs in different ionic strengths (NaCl).

360 nm to 460 nm. The shape of the emission spectrum and the position of the peak did not change significantly at different excitation wavelengths, but the fluorescence intensity changed a lot (Fig. 2c), suggesting π-π^* transition [27]. At an excitation wavelength of 440 nm, the N, S-CDs resolved in solutions emitted a maximum wavelength of 520 nm. The QY of N, S-CDs in water reached 37.2% (Fig. S1 in Supporting information), which made N, S-CDs potential bioimaging agents. The high QY may be owed to that the aromatic structure contained in N, S-CDs can form large π-conjugated structure and the amino group on the surface of N, S-CDs further increases the degree of conjugation and enhances the probability of the transition of the ground state electron to the lowest excited state [28,29]. The photoluminescence mechanism of N, S-CDs may be owed to the absorption bands from the n-π^* transition of the aromatic sp^2 system containing C=O and C=N bonds [30]. Meanwhile, surface passivation and local heteratom doping were considered as a potential mechanism to enhance the quantum yield of N, S-CDs [31]. The fluorescence decay of N, S-CDs was 7.32 ns (Fig. S2 in Supporting information).

The fluorescence intensity of the carbon dots can be influenced by various factors (*e.g.*, metal ion [32] and pH alterations [33]) However, for excellent bioimaging, fluorescence should remain stable when affected by external conditions. The N, S-CDs were very stable over time as shown in Fig. S3 (Supporting information). Meanwhile, the photoluminescence spectra of N, S-CDs at different pH values were described in Fig. 2d and Fig. S4 (Supporting information). N, S-CDs' fluorescence remained stable and strong in a wide pH range (3 – 9), suggesting that N, S-CDs could be applied in acid/alkaline contexts. The impact of pH on photoluminescence could be illustrated by the deprotonation caused by acid and alkali leading to the surface charge change of N, S-CDs [34]. Furthermore, the N, S-CDs were treated with solutions of different ionic

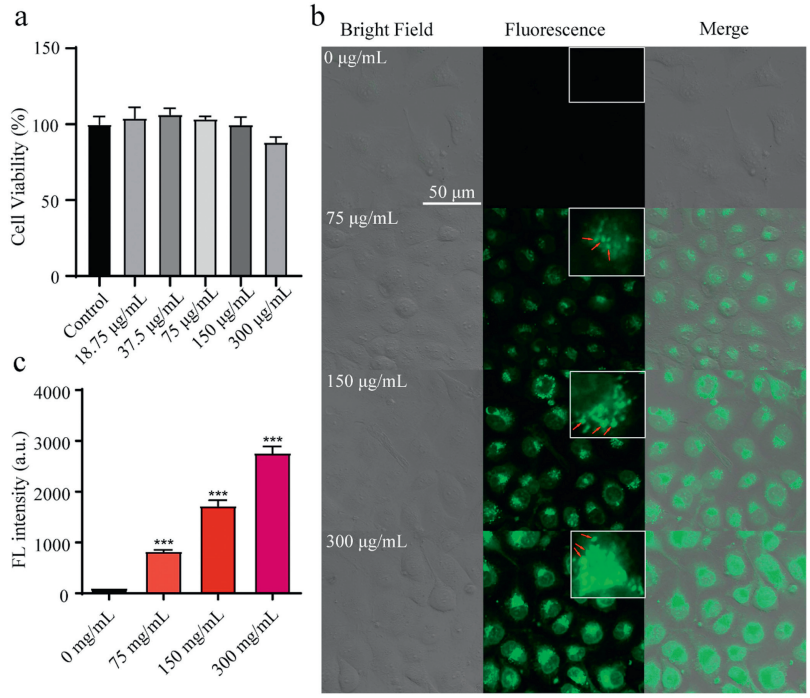

Fig. 3. (a) Cell viability of HUVEC cells by incubation with different concentrations of N, S-CDs. (b) Confocal imaging of HUVEC cells with different concentrations of N, S-CDs and without carbon, the red arrow indicates carbon dots. (c) The mean fluorescence intensity of HUVEC cells after incubation with different concentrations of N, S-CDs was calculated based on the flow cytometer data in Fig. S5, data are represented as mean ± SD ($n = 3$).

strengths (10^{-7}~10^{-1} mol/L) or exposed to ultraviolet light (365 nm) for different time periods, the fluorescence intensity of N, S-CDs remained stable. The corresponding results were shown in Figs. 2e and f.

To be a fluorescent nano-material for biological applications, it is also necessary to be of low toxicity. Therefore, the MTT assay was conducted to investigate the cytotoxicity of N, S-CDs and the corresponding result was shown in Fig. 3a. Cell viability of HUVEC did not change evidently among gradient concentrations of N, S-CDs (up to 300 μg/mL), and the cell viability kept more than 90% compared with control even under the highest concentration of N, S-CDs, indicating N, S-CDs has low cytotoxicity.

To investigate the cell uptake potential of N, S-CDs, HUVEC cells were incubated with different concentrations of N, S-CDs for 6 h at 37 °C. According to the results of confocal fluorescence imaging, N, S-CDs could be uptaken by HUVEC cells and mainly existed in the cytoplasm but not in the nucleus (Fig. 3b). In addition, with the increase of concentrations of the N, S-CDs, the fluorescence intensity in the cytoplasm also simultaneously increased, which was similar to most nanoparticles [35,36]. Besides, the flow cytometry was also engaged to assess the uptake efficiency of N, S-CDs by HUVEC cells (Fig. S5 in Supporting information). As shown in Fig. 3c, the mean fluorescence gradually enhanced with increased concentrations of N, S-CDs. The results confirmed that the uptake of N, S-CDs was concentration-dependent. The mechanism by which N, S-CDs were taken up by HUVEC cells was further explored. According to previous studies, the surface chemistry, particle size, hydrophilicity or hydrophobicity of nanoparticles can affect their internalization pathway [37]. Typically, nanoprobe was taken up by cells mainly through various endocytic pathways, such as phagocytosis, micropinocytosis, clathrin- and caveolin-mediated endocytosis [38]. To explore the mechanism by which N, S-CDs were taken up by HUVEC, HUVEC were pretreated with multiple inhibitors. NaN_3 is an inhibitor of all energy-dependent endocytosis. Colchicine can prevent the formation of caveolae. Nystatin inhibits the caveolae and lipid raft endocytic pathway Chlorpromazine can disrupt the clathrin vesicles formation. Amiloride can inhibit micropinocytosis. The uptake efficiency of N, S-CDs was detected by flow and confocal (Fig. 4). The results revealed that these inhibitors have no significant effect on cellular internalization of N, S-CDs. This may be owed to the fact that the N, S-CDs penetrate the lipid bilayer of the cell membrane into the cytoplasm [39], which demonstrated that the N, S-CDs crosses the cell membrane *via* an energy-independent manner and exhibited excellent cell-penetrating ability.

The blood compatibility of biomaterials is another important criterion for evaluating their safety when participated in the systemic circulation. Evaluation principles commonly used for blood compatibility include hemolysis rate, erythrocyte aggregation and morphological changes [20]. The hemolysis results after erythrocyte incubated with gradient concentrations of N, S-CDs were presented in Fig. 5a. Apparent hemolysis was observed in control group (TritonX-100). While the solution supernatants were colorless after treatments with gradient concentrations of N, S-CDs, suggesting no evident hemolysis-phenomenon come up. The results of the hemolysis rate were displayed in Fig. 5b. Whether the incubation time was 2 or 4 h, the hemolysis rate was always lower than 0.5% at different concentrations. Besides, the accumulation of erythrocytes may cause vascular occlusion, which likely further accounts for more severe diseases. So we checked the dispersion and morphology of erythrocytes by scanning electron microscopy (SEM). As shown in Fig. 5c, the erythrocyte treated with N, S-CDs were uniformly dispersed and the morphology had no alteration and accumulation as similar to the control group. According to the hemolysis results, it can be concluded that N, S-CDs had good blood compatibility for potential bioimaging use *in vivo*.

In summary, we synthesized the green fluorescent N, S-CDs *via* a simple one-step method. The TEM image illustrated that N, S-CDs possessed excellent dispersibility and uniform particle size in solutions. Meanwhile, the N, S-CDs had high QY (37.2%). *In vitro*, N,

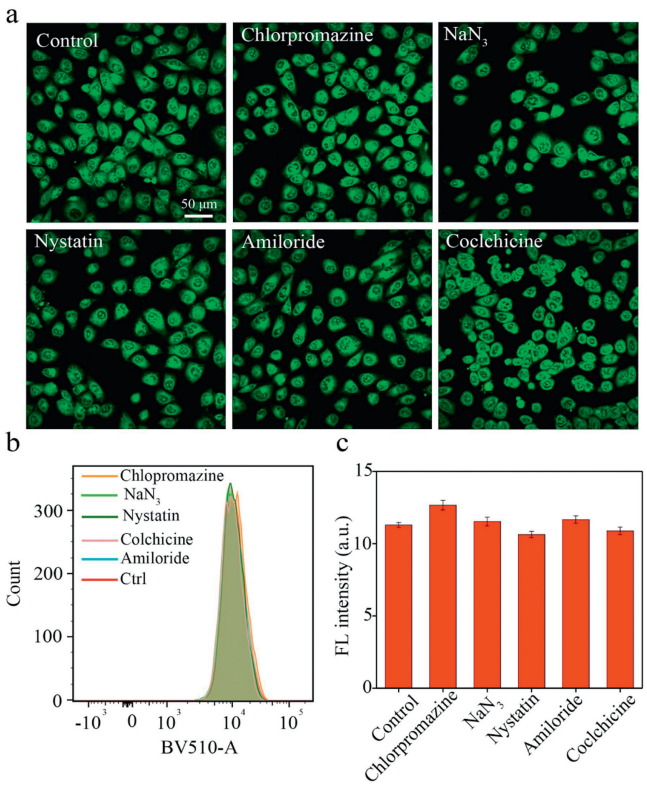

Fig. 4. (a) Confocal images of HUVEC cells were incubated with 300 μg/mL N, S-CDs for 3 h and pretreated with different inhibitors. (b) The fluorescence of HUVEC cells were quantified by flow cytometer. (c) The fluorescence intensity of HUVEC cells after incubation with different concentrations of N, S-CDs was calculated based on the flow cytometer (data are represented as mean ± SD, $n = 3$).

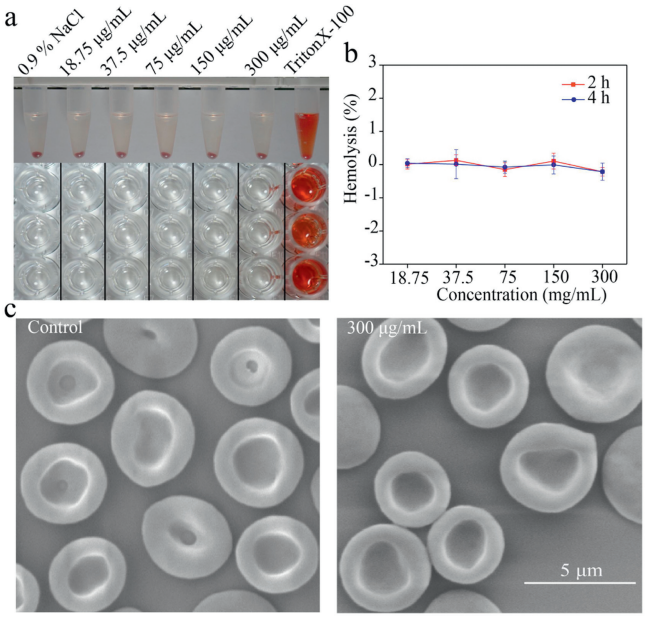

Fig. 5. (a) Hemolysis observation after incubation of different concentrations of N, S-CDs with 0.2% erythrocyte for 2 h. (b) Hemolysis rate of different concentrations of N, S-CDs at 2 and 4 h. (c) Scanning electron microscopy (SEM) image of erythrocyte treated with N, S-CDs.

S-CDs showed almost no cytotoxicity to HUVECs and confocal microscopy as well as flow analysis showed that N, S-CDs could be efficiently taken up by HUVECs and localize in the cytoplasm of HUVECs. Moreover, the hemolysis rates caused by treatments of different N, S-CDs concentrations were below 0.5%. The morphology of erythrocyte did not change and no accumulation after N, S-CDs treatment, indicating that N, S-CDs displayed good blood compatibility. The N, S-CDs have promising prospects for *in vivo* imaging.

Declaration of competing interest

The authors declare that they have no known competing financial interests or personal relationships that could have appeared to influence the work reported in this paper.

Acknowledgments

This research was supported by the National Key Specialty Construction Project of Clinical Pharmacy (No. 30305030698) and Research Funding of Sichuan Provincial People's Hospital (Nos. 2018LY06, 2017LY08). We would like to thank Mei Chen and Peng Yang for their technical support.

Appendix A. Supplementary data

Supplementary material related to this article can be found, in the online version, at doi:https://doi.org/10.1016/j.cclet.2020.01.007.

References

[1] S. Zhu, Y. Song, X. Zhao, et al., Nano Res. 8 (2015) 355–381.
[2] X. Xiao, R. Robert, G. Yun, et al., J. Am. Chem. Soc. 126 (2015) 12736–12737.
[3] S. Yang, H. Gao, Pharmacol. Res. 126 (2017) 97–108.
[4] V. Georgakilas, J.A. Perman, J. Tucek, et al., Chem. Rev. 115 (2015) 4744–4822.
[5] X. Miao, D. Qu, D. Yang, et al., Adv. Mater. 30 (2018) 1704740.
[6] T. Feng, X. Ai, G. An, et al., ACS Nano. 10 (2016) 4410–4420.
[7] Q. Xu, M. Xu, C.Y. Lin, et al., Adv. Sci. 6 (2019) 1902043.
[8] S.N. Baker, G.A. Baker, Angew. Chem. Int. Ed. 49 (2010) 6726–6744.
[9] U. Reschgenger, M. Grabolle, S. Cavalierejaricot, et al., Nat. Methods 5 (2008) 763–775.
[10] Z. Li, T. Liu, J. Long, et al., Chin. Chem. Lett. 30 (2019) 582–586.
[11] X. Shi, H. Meng, Y. Sun, et al., Small 15 (2019) 1901507.
[12] S. Lu, L. Sui, J. Liu, et al., Adv. Mater. 29 (2017) 1603443.
[13] W. Xiao, Y. Li, C. Hu, et al., J. Colloid Interface Sci. 497 (2017) 226–232.
[14] Q. Guan, J. Ma, W. Yang, et al., Nanoscale 11 (2019) 14123–14133.
[15] Y. Yang, X. Ren, Z. Sun, et al., Chin. Chem. Lett. 29 (2018) 895–898.
[16] W. Li, Y. Liu, B. Wang, et al., Chin. Chem. Lett. 30 (2019) 2323–2327.
[17] M. Zhang, R. Su, J. Zhong, et al., Nano Res. 12 (2019) 815–821.
[18] Y. Cao, Y. Gong, L. Liu, et al., J. Appl. Toxicol. 37 (2017) 1359–1369.
[19] B.I. Cerda-Cristerna, H. Flores, A. Pozos-Guillén, et al., J. Control. Release 153 (2011) 269–277.
[20] L. Cheng, Y. Li, X. Zhai, et al., ACS Appl. Mater. Interfaces 6 (2014) 20487–20497.
[21] J.L. Fajardo-Díaz, F. López-Urías, E. Muñoz-Sandoval, Sci. Rep. 8 (2018) 3546.
[22] J. Li, G. Zuo, X. Pan, et al., Luminescence 33 (2018) 243–248.
[23] N.A. Travlou, D.A. Giannakoudakis, M. Algarra, et al., ACS Appl. Mater. Interfaces 10 (2018) 10664–10677.
[24] C. Shi, H. Qi, R. Ma, et al., Mater. Sci. Eng. 105 (2019) 110132.
[25] X. Hua, Y. Bao, F. Wu, ACS Appl. Mater. Interfaces 10 (2018) 10664–10677.
[26] S. Tao, S. Lu, Y. Geng, et al., Angew. Chem. Int. Ed. 57 (2018) 2393–2398.
[27] Y. Jiao, X. Gong, H. Han, et al., Anal. Chim. Acta 1042 (2018) 125–132.
[28] Y. Dong, H. Pang, H.B. Yang, et al., Ange. Chem. Int. Ed. 52 (2013) 7800–7804.
[29] H. Liu, Z. Li, Y. Sun, et al., Sci. Rep. 8 (2018) 1086.
[30] X. Miao, D. Qu, D. Yang, et al., Adv. Mater. 30 (2018) 1704740.
[31] W. Cai, T. Zhang, M. Xu, et al., J. Mater. Chem. C 7 (2019) 2212–2218.
[32] C. Li, W. Liu, Y. Ren, et al., Sen. Actuators B 240 (2017) 941–948.
[33] Y. Ding, X. Gong, Y. Liu, et al., Talanta 189 (2018) 8–15.
[34] J. Li, G. Zuo, X. Pan, et al., Luminescence 33 (2018) 243–248.
[35] H. Gao, Z. Pang, L. Fan, et al., Acta Pharmacol. Sin. 31 (2010) 237–243.
[36] J. Qian, J. Chen, S. Ruan, et al., J. Colloid Interface Sci. 429 (2014) 77–82.
[37] A. Chakraborty, N. Jana, J. Phys. Chem. Lett. 6 (2015) 3688–3697.
[38] W. Guo, F. Pi, H. Zhang, et al., Biosens. Bioelectron. 98 (2017) 299–304.
[39] J. Chen, X. Zhang, Y. Zhang, et al., Langmuir 33 (2017) 10259–10270.